



Stratospheric chlorine processing after the 2020 Australian wildfires derived from satellite data

Peidong Wang^{a,1}, Susan Solomon^a, and Kane Stone^a

Edited by Paul Wennberg, California Institute of Technology, Pasadena, CA; received August 12, 2022; accepted February 3, 2023

The 2019 to 2020 Australian summer wildfires injected an amount of organic gases and particles into the stratosphere unprecedented in the satellite record since 2002, causing large unexpected changes in HCl and ClONO₂. These fires provided a novel opportunity to evaluate heterogeneous reactions on organic aerosols in the context of stratospheric chlorine and ozone depletion chemistry. It has long been known that heterogeneous chlorine (Cl) activation occurs on the polar stratospheric clouds (PSCs; liquid and solid particles containing water, sulfuric acid, and in some cases nitric acid) that are found in the stratosphere, but these are only effective for ozone depletion chemistry at temperatures below about 195 K (i.e., largely in the polar regions during winter). Here, we develop an approach to quantitatively assess atmospheric evidence for these reactions using satellite data for both the polar (65 to 90°S) and the midlatitude (40 to 55°S) regions. We show that heterogeneous reactions apparently even happened at temperatures at 220 K during austral autumn on the organic aerosols present in 2020 in both regions, in contrast to earlier years. Further, increased variability in HCl was also found after the wildfires, suggesting diverse chemical properties among the 2020 aerosols. We also confirm the expectation based upon laboratory studies that heterogeneous Cl activation has a strong dependence upon water vapor partial pressure and hence atmospheric altitude, becoming much faster close to the tropopause. Our analysis improves the understanding of heterogeneous reactions that are important for stratospheric ozone chemistry under both background and wildfire conditions.

stratospheric ozone | chlorine activation | wildfire

The Australian wildfire black summer was the largest such event in the satellite era. It produced on the order of 1 Tg of aerosols in the stratosphere from about December 31, 2019, to January 5, 2020 (1), equivalent to a small volcanic eruption. These aerosols and their precursors are brought into the lower stratosphere by pyrocumulonimbus convection, where they can be expected to decay over time. Volcanic aerosols typically display an e-folding time of about 18 mo (2, 3). Model simulations (which assumed wildfire-released aerosols behave like sulfuric acid and water particles) (4), satellite observations (5–7), and in situ measurements (8) all found significant ozone decreases in the lower stratosphere at southern hemisphere midlatitudes in 2020 after the wildfire. Unusually low ozone abundances even continued into 2021 (6, 9). While there is evidence for some dynamical contributions to the ozone variations observed in that year (6, 10), averaged midlatitude values presented in ref. 6 indicate record low local abundances near 20 km, suggesting additional chemistry is likely. In addition, unprecedented and completely unexpected changes in midlatitude chlorine (Cl) reservoir species (HCl and ClONO₂) were also found in satellite and in situ observations (6–8), suggestive of Cl surface chemistry. In the polar region, the following heterogeneous reaction $\text{HCl} + \text{ClONO}_2 \rightarrow \text{Cl}_2 + \text{HNO}_3$ (11) occurs at cold temperatures. The Cl₂ subsequently photolyzes rapidly in sunlit air and can form Cl and ClO which deplete ozone. Other reactions are possible, such as $\text{HOCl} + \text{HCl} \rightarrow \text{Cl}_2 + \text{H}_2\text{O}$ but our observational analysis does not allow us to determine what reactions are occurring. It is plausible that organic aerosols may drive similar reactions at warmer temperatures (discussed in detail below). The fingerprint of N₂O₅ hydrolysis, another key heterogeneous reaction that contributes to depletion in the ozone layer, was also found in the satellite data (12) but cannot explain the unusual changes in HCl and ClONO₂. Here we provide a fresh approach to the analysis of the Cl chemistry inspired by the unexpected HCl and ClONO₂ data that sheds light on its temperature-dependent chemistry not only for wildfires but also for background conditions. However, this work will not quantify the ozone loss and will be exclusively focused on the Cl chemistry.

Laboratory measurements (13, 14), in situ observations (15), and model simulation (16) all suggest that the heterogeneous Cl reaction between HCl and ClONO₂ is only effective on the surfaces of typical stratospheric aerosols at temperatures below 195 K.

Significance

Heterogeneous chlorine activation is a major driver for stratospheric ozone depletion and is understood to happen on polar stratospheric clouds (PSCs) at temperatures below about 195 K. The 2020 Australian wildfire released large amounts of organic aerosols, whose chemical properties under stratospheric conditions are virtually unknown. Here, we developed an approach to analyze the temperature dependency of atmospheric chlorine heterogeneous chemistry using satellite data. We found that such reactions can happen at temperatures even at 220 K on wildfire aerosols in 2020. Organic aerosols are present to some degree in the lower stratosphere even under background conditions. This result indicates that Cl processes on organic aerosols likely need to be considered in future stratospheric ozone simulations.

Author affiliations: ^aDepartment of Earth, Atmospheric, and Planetary Sciences, Massachusetts Institute of Technology, Cambridge, MA 02139

Author contributions: P.W. and S.S. designed research; P.W. and K.S. performed research; P.W. analyzed data; and P.W., S.S., and K.S. wrote the paper.

The authors declare no competing interest.

This article is a PNAS Direct Submission.

Copyright © 2023 the Author(s). Published by PNAS. This open access article is distributed under [Creative Commons Attribution-NonCommercial-NoDerivatives License 4.0 \(CC BY-NC-ND\)](https://creativecommons.org/licenses/by-nc-nd/4.0/).

¹To whom correspondence may be addressed. Email: pdwang@mit.edu.

This article contains supporting information online at <https://www.pnas.org/lookup/suppl/doi:10.1073/pnas.2213910120/-/DCSupplemental>.

Published March 6, 2023.

In contrast to stratospheric background sulfuric acid and water aerosols, wildfire-released particles contain a wide variety of organic compounds (17, 18), which could have different chemical properties. Limited laboratory studies suggest that organic aerosols can enhance HCl uptake (19) and at warmer temperatures (20).

The approach presented here quantifies the temperature for Cl activation using satellite data from Atmospheric Chemistry Experiment-Fourier Transform Spectrometer (ACE-FTS; ACE for short) (21) combined with temperatures from a back trajectory model named Lagranto (Lagrangian Analysis Tool) (22), driven by meteorological conditions from ERA5 reanalysis data (fifth generation atmospheric reanalysis product from the European Centre for Medium-Range Weather Forecasts) (23). We focus on the southern hemisphere midlatitudes defined as 40 to 55°S and the polar vortex region defined as 65 to 90°S. The most significant changes in HCl and ClONO₂ in 2020 are observed at altitudes ranging between 15 and 22 km in 40 to 60°S (*SI Appendix, Fig. S1*). Unless otherwise specified, we mainly focus on 18.5 km in our analysis to maximize the effects.

Results

Separating Dynamical and Chemical Processes. Fig. 1*A* shows the monthly mean ACE data for CO (an indicator of biomass burning) at the lower stratosphere midlatitudes. Record high CO in 2020 (6, 7) was observed immediately after the pyrocumulonimbus events in January and decayed with time, suggesting a significant amount of biomass burning and its long-lasting effect continuing throughout the entire year. CO in 2021 is within the range of climatology, indicating no significant wildfire or new particles injected into the lower stratosphere in that year. Year 2012 is also highlighted in Fig. 1 since we use it here as a typical reference year in later analysis, given no known large volcanic eruptions nor big biomass burning events in that year.

While HCl displayed remarkable anomalies in 2020, HF was within the range of past years, confirming the role of chemistry

(Fig. 1). Once anthropogenically produced chlorofluorocarbons (CFCs) reach the stratosphere, they decompose into the fluorine (Fy) and chlorine (Cly) families of compounds. Nearly all of the Fy is in the form of HF because there are no known chemical loss pathways of HF in the stratosphere; hence it has long been used as an inactive tracer (24, 25). Insofar as the breakdown of CFCs is the dominant source of both stratospheric chlorine and fluorine, Cly and Fy should be proportional to one another. Viewed in this context, HCl and HF behavior also suggests unusual chemistry lasting into 2021, but with much smaller magnitude than 2020.

Correlation between chemical species or “tracer–tracer” analysis is a powerful tool to analyze dynamical and chemical interactions (26–28). The basis of the analysis is that dynamical transport should affect inactive and active species similarly, so departures from correlation in the active species are indicative of chemical processes. The availability of simultaneous ACE observations of HF, HCl, and ClONO₂ along a common line of sight ensures consistency and is key to such an analysis. To separate dynamical from chemical effects on specific Cly species, we perform the tracer–tracer analysis between HF and HCl, ClONO₂, and their sum (Fig. 2 for midlatitude and *SI Appendix, Fig. S2* for the polar region).

Fig. 2 and *SI Appendix, Fig. S2* show tracer–tracer scatter plots of ACE HF and HCl, ClONO₂, and HCl+ClONO₂ in each month from March to July at the midlatitudes (40 to 55°S) and polar vortex region (65 to 90°S), respectively. We focus on months between March and July because in the polar vortex region, this spans months when no or little heterogeneous chemistry normally occurs (~March to April) to months with rapid chemistry on polarstratospheric clouds (PSCs) (June to July) and in between (May). All the data align on a nearly straight line in March, suggesting little or no chemistry in this month. We therefore construct a baseline relationship between HF and the Cly species from March 2004 to 2019 data using linear regression (indicated by the dark solid lines in Fig. 2 and *SI Appendix, Fig. S2*).

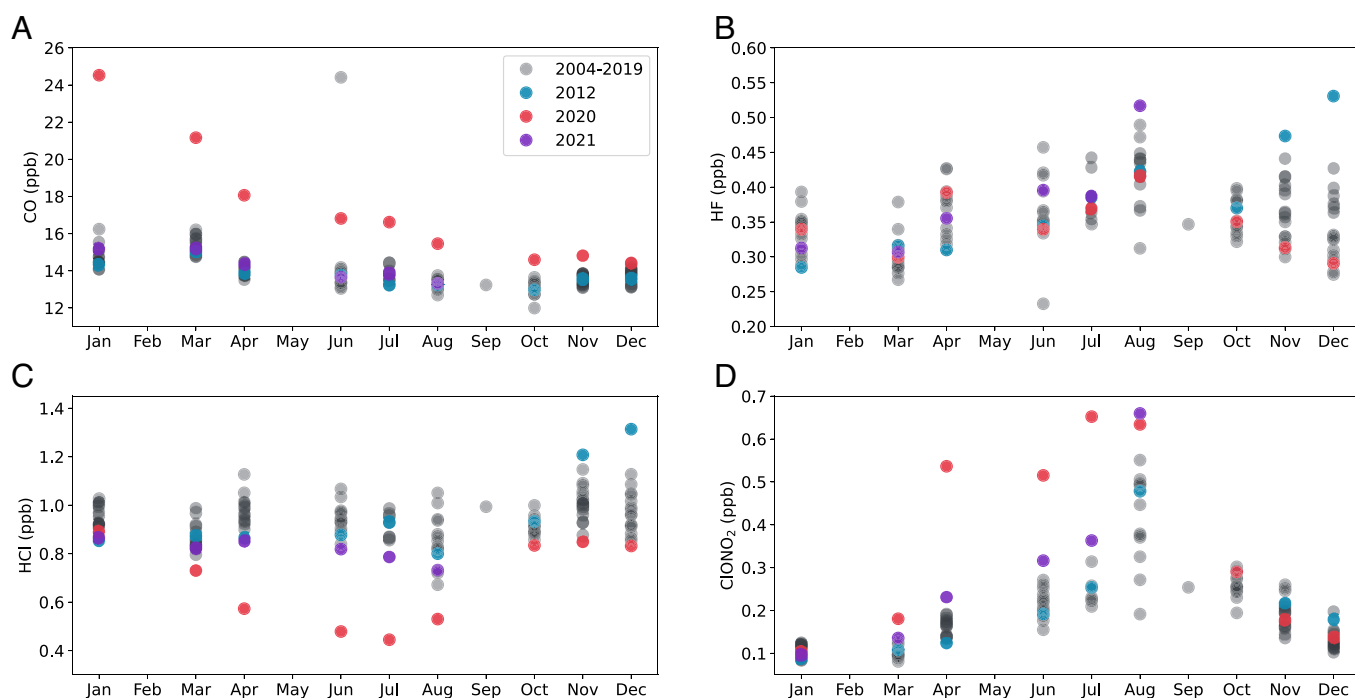


Fig. 1. The monthly mean ACE data for (A) CO, (B) HF, (C) HCl, and (D) ClONO₂ at 18.5 km averaged over 40 to 55°S. Red dots are from 2020, purple dots are from 2021, blue dots are from 2012 (used as a reference year in this study), and gray dots are from 2004 to 2019 (excluding 2012); 40 to 55°S is split into three equally spaced latitude bins and months with at least five samples (at least one sample per latitude bin) are considered in the averaging processes.

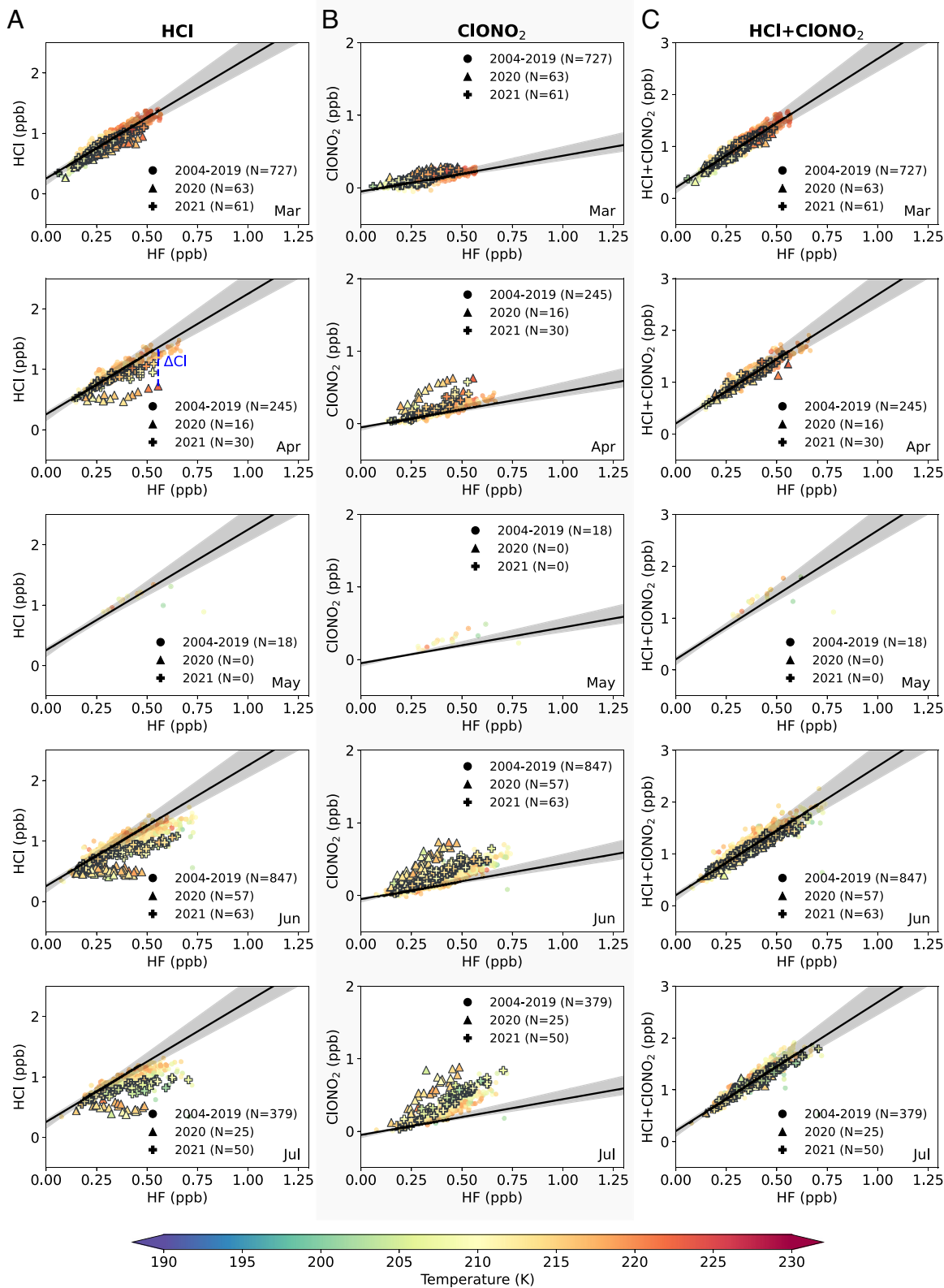


Fig. 2. Tracer-tracer correlation between ACE-measured HF (x axis) and (A) HCl, (B) ClONO₂, and (C) HCl+ClONO₂ (y axes), color-coded by temperature. Each dot represents a single measurement at 18.5 km over 40 to 55°S. Dots in 2020 and 2021 are highlighted with triangles and crosses, respectively (with gray edges). Each subpanel shows a different month from March to July, labeled at the bottom right corner. The number of data plotted in each month is shown in the legend. The thick black lines represent the no-chemistry baseline, from the linear fit over March 2004 to 2019 data points. The shaded regions indicate a conservative full range of baseline variability bounded by the maximum and minimum baselines constructed by data in individual years from 2004 to 2019. A demonstration of how Δ Cl (e.g., in Fig. 4) is calculated is shown here as the vertical blue dashed line in the April panel for HCl, representing the change in Cl due to chemical processes.

The shaded regions in Fig. 2 and *SI Appendix, Fig. S2* quantify the baseline uncertainty. There are mainly two types of uncertainties in such analysis, one is the instrumental bias, and the other is the

interannual variability. As the tracer-tracer correlation mainly focuses on the relative difference of Cly to HF, which are measured by ACE at the same occultation, instrumental bias on both

molecules will largely cancel. To quantify the uncertainty of inter-annual variability and noise, we construct a baseline for each year in 2004 to 2019 to represent the range of variability in baselines. The shading areas indicate a conservative full range of variability bounded by the maximum and minimum baselines using data in individual years.

ACE has limited data coverage. To validate whether the results are robust, we compare ACE (at 18.5 km) with the Microwave Limb Sounder (MLS at 68.2 hPa) in *SI Appendix, Figs. S3 and S4* (midlatitude and polar vortex region, respectively) for tracer–tracer analysis between N_2O and HCl (since MLS does not have measurements for HF and $ClONO_2$). MLS has much more spatial coverage, but with a lower signal-to-noise ratio on individual points (as shown in *SI Appendix, Figs. S3C and S4C*). The zonally averaged MLS data (*SI Appendix, Figs. S3B and S4B*) agree well with ACE (*SI Appendix, Figs. S3A and S4A*), suggesting that even though ACE coverage is limited, it is consistent with MLS regarding the changes in HCl from tracer–tracer analysis. Note that the zonal averaging process in MLS reduces the noise, but it also clusters measurements toward the mean values. Therefore, the baseline slope becomes more sensitive to small changes in N_2O and HCl in the clustered region, and the uncertainty range expands at those values where no or few data are fed into the linear regression. MLS N_2O also has experienced a $\sim 3\%$ instrumental drift in the past decade, which could also broaden the spread of the baseline uncertainty range (29). We therefore focus on the results from ACE measurements.

In the polar vortex region, *SI Appendix, Fig. S2* shows that substantial deviations in HCl and $ClONO_2$ from their respective “no-chemistry” baseline occur in July for every year, indicating the known Cl activation mechanism on PSCs (11). Over the mid-latitudes (Fig. 2), some data points in June and July from 2004 to 2019 fall off the no-chemistry baseline. However, 2020 data points in the midlatitude region in these 2 mo are completely outside the range of climatology. More important, in 2020, HCl and $ClONO_2$ start to deviate from the no-chemistry baseline even in April in both midlatitude and polar regions, when the temperature is far too warm for heterogeneous Cl reactions to happen. HCl and $ClONO_2$ in 2021 also display some deviations from the no-chemistry baseline, but the magnitudes are considerably smaller than in 2020.

Interestingly, the decrease in HCl is roughly compensated by increases in $ClONO_2$ in both 2020 and 2021 (e.g., April and May in Fig. 2 and *SI Appendix, Fig. S2*, respectively) and in other years.

The decrease in HCl suggests that anomalous heterogeneous Cl reactions occurred in these 2 y. However, at these latitudes outside the polar vortex, ample solar radiation is available to drive HNO_3 photolysis (and reaction with OH also occurs), making NO_2 available to deactivate the activated Cl, forming $ClONO_2$. With a rich supply of NO_2 , the net reaction thus largely transfers HCl into $ClONO_2$. Similar Cl deactivation forms the $ClONO_2$ “collar” (30), a slice of enhanced $ClONO_2$ surrounding the polar vortex in late spring as noted in past literature. Fig. 3 shows May HCl and $ClONO_2$ anomalies in 2020 compared to the May climatology from 2004 to 2019. The figure makes clear that the $ClONO_2$ collar mechanism is significantly enhanced in 2020 as early as May, as more Cl has been converted from HCl into $ClONO_2$ apparently on wildfire-released particles. Similar processes continued to occur in 2021, but with a smaller magnitude (*SI Appendix, Fig. S5*). HCl and $ClONO_2$ are both considered to be reservoirs for active chlorine species that deplete ozone (mainly Cl and ClO). It may be useful to consider such a process to represent Cl processing instead of Cl activation, since the sum of $HCl+ClONO_2$ is nearly conserved. Nonetheless, a small amount of enhanced ClO will be present as well, since $ClONO_2$ and ClO are essentially in photochemical balance in the sunlit atmosphere, and enhanced $ClONO_2$ therefore implies enhanced ClO and associated ozone loss. Indeed, the evidence of enhanced ClO has been shown in both ACE and MLS measurements (6, 7).

Cl Processing in the Midlatitudes. To estimate the temperatures that are likely to drive the heterogeneous chemistry, we first calculate the deviation of each data point in Fig. 2 from the no-chemistry baseline as a function of ACE-measured temperature (Fig. 4 A–C). Thick lines show the averages of data points in 2 K temperature bins from the baseline that is constructed by all available data from 2004 to 2019. The shaded regions represent the full range of Cl deviation from individual no-chemistry baselines that are constructed from data in individual years, representing the uncertainty due to variability. Negative values in $ClONO_2$ at warmer temperatures indicate that available ClO has been deactivated to form $ClONO_2$, and the sum of HCl and $ClONO_2$ in Fig. 4C thus indicates that a large amount of the Cl activated from HCl in 2020 and 2021 has almost all formed $ClONO_2$ at warmer temperatures. As we focus on 40 to 55°S where the temperature is well above 195 K, activation on the PSCs is not likely to take place. This is supported by the 2004 to 2019 climatology, in which the average Cl activation remains

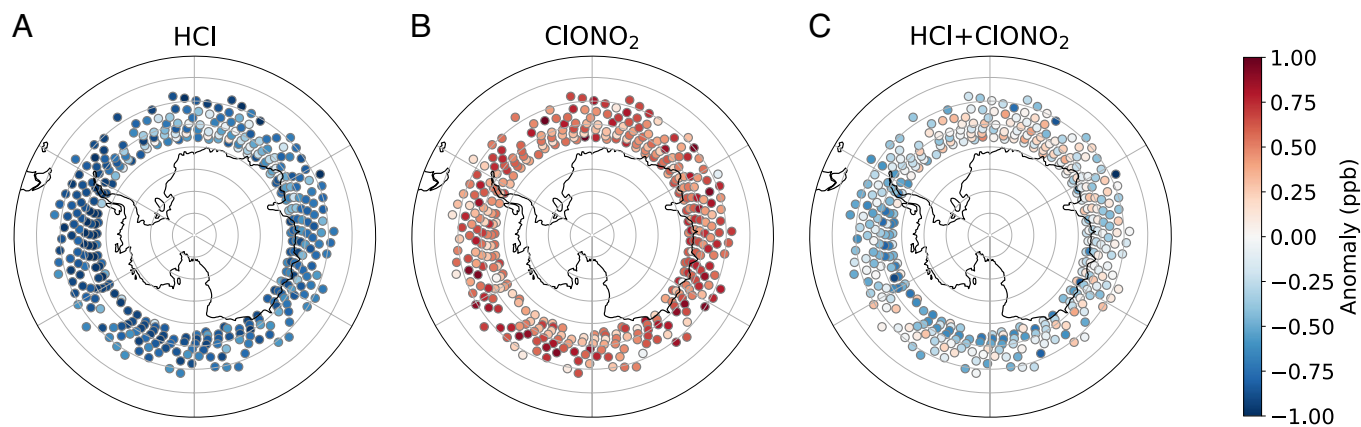


Fig. 3. Monthly anomalies for (A) HCl, (B) $ClONO_2$, and (C) $HCl+ClONO_2$ in May 2020 compared to the May climatology in 2004 to 2019. The maps show a latitudinal range between 50 and 90°S since ACE measurements in May are mainly between 58 and 68°S. To prevent from biasing the anomalies by latitudinal variations, the climatological mean is constructed at every 5° latitude bin. Therefore, the May anomalies presented here are calculated from four latitude bins from the climatology (50 to 55, 55 to 60, 60 to 65, and 65 to 70°S).

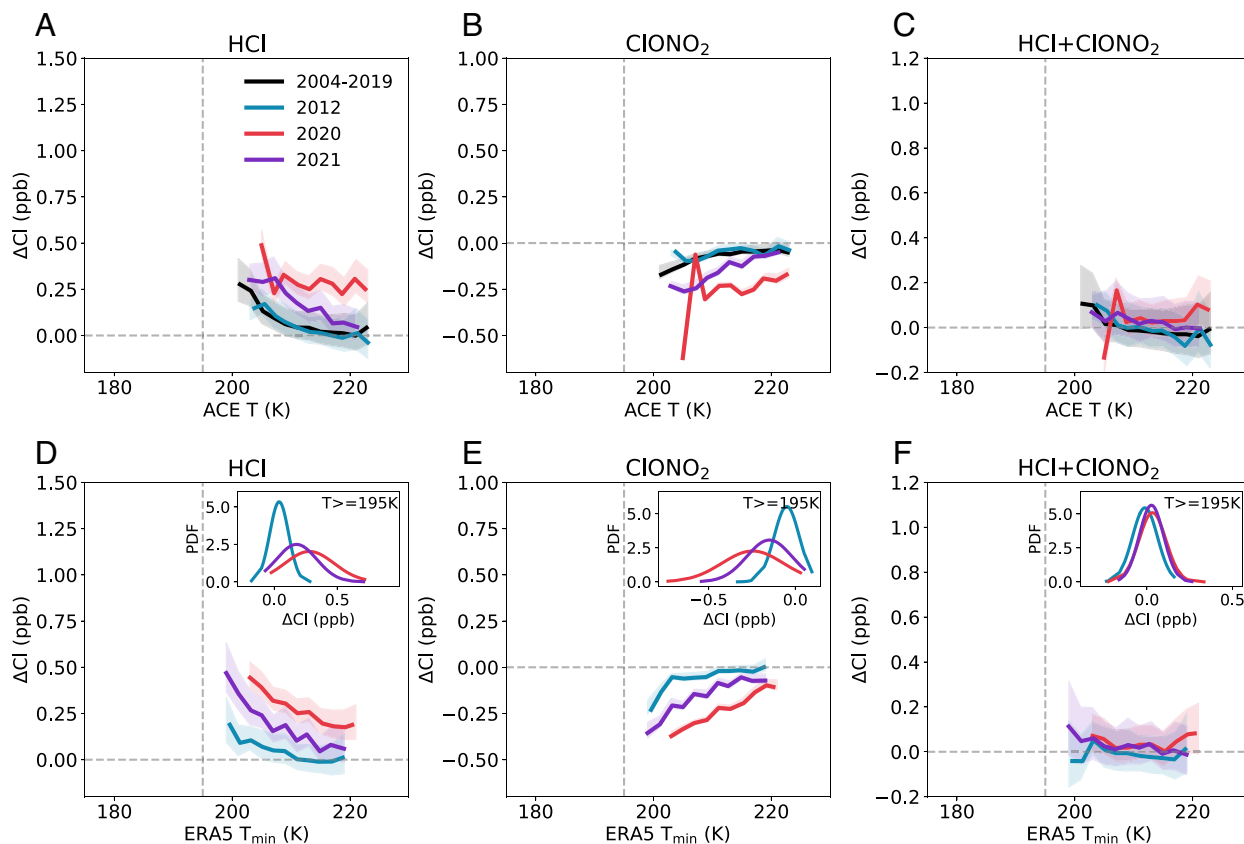


Fig. 4 Cl activation as a function of temperature at midlatitudes (40 to 55°S) for March to July at 18.5 km. Each panel shows the amount of Cl activation on the y axes (deviation from the no-chemistry baseline in Fig. 2) as a function of temperature (x axis) for (A and D) HCl, (B and E) ClONO₂, and (C and F) HCl+ClONO₂. Panels A–C use the ACE-measured temperature at the satellite overpass, and panels D–F use the minimum temperature (T_{\min}) calculated along the 5-d back trajectories for each data point for 2020, 2021, and 2012. Thick lines are the average of Cl activation at every 2 K temperature bins (temperature bins with less than two samples are not considered for the average). The shading areas indicate the full range of Cl departures from individual baselines using data from single years. Horizontal and vertical gray dashed lines indicate zero Cl activation and 195 K, respectively. The probability distribution functions (PDF) of Cl activation at $T_{\min} \geq 195$ K are shown in panels D–F for 2020, 2021, and 2012.

close to zero. However, HCl data in 2020 and 2021 suggest that significant Cl activation occurred at temperatures even well above 200 K, but not in any other years (although the magnitude of Cl activation in 2021 is smaller than in 2020).

However, one pitfall of Figs. 2 and 4 A–C is that the temperatures shown reflect only the state of the atmosphere at the satellite overpass, while Cl activation could have occurred at a different temperature along air parcel trajectories. We therefore use Lagranto (22) driven by ERA5 (23) to evaluate 5-d kinematic back trajectories for each data point in 2020 and 2021, as well as the reference year of 2012. Like all trajectory studies, errors in wind, temperature, and parcel motion cannot be eliminated in our analysis and are a source of uncertainty in the detailed chlorine activation estimates versus temperature. Lagranto calculates the kinematic trajectories, but air parcels likely travel adiabatically or may cross isentropes due to diabatic processes (such as local heating due for example to particles absorbing more radiation). The radiative relaxation time for the lower stratosphere is on the order of 20 to 30 d (31, 32); we pick a rather conservative estimate of 5 d to avoid potential effects of radiatively driven ascent/descent of particles in the stratosphere. The ACE-measured instantaneous temperature is then replaced with the minimum temperature from the 5-d back trajectories of each data point (referred to as ERA5 T_{\min} in Fig. 4 D–F), providing an estimate of the air parcel’s recent minimum temperature exposure. ERA5 temperatures at the collocated ACE observations agree well with each other (SI Appendix, Fig. S6), and we find that the 5-d minimum temperature is rather insensitive to small perturbations in the starting position (SI Appendix, Fig. S7).

Fig. 4 D–F shows Cl activation as a function of the 5-d minimum temperature calculated from Lagranto. The 5-d minimum temperature exposure for these measurements is still mainly above 195 K. This further strengthens the idea that wildfire-released organic aerosols can allow heterogeneous reactions to happen at warmer temperatures, which differs from the PSC mechanism limited in the polar region that requires the temperature to be lower than 195 K. Further, the probability distribution functions (PDFs) shown in Fig. 4 D–F for temperatures ≥ 195 K indicate that not only do 2020 and 2021 have different mean values than in 2012, but the spread after the wildfire is also much wider than that in 2012. One plausible explanation for this behavior is variability in the composition and/or abundances of organic aerosols from the wildfire, displaying different chemical properties. Note that the PDF for the sum of HCl+ClONO₂ is centered very close to zero for 2012 (-0.01 ± 0.07 ppb; \pm sign followed by one SD) and displays a slight offset from zero in 2020 and 2021 (0.03 ± 0.08 ppb and 0.03 ± 0.07 ppb, respectively), indicating small but non-negligible enhancements in other species including HOCl (7) and ClO in those years only (6), given the changes in the latter two species can be few orders of magnitude smaller than changes in HCl and ClONO₂.

Cl Processing in the Polar Vortex Region. Fig. 5 shows Cl activation in the polar vortex region at 65 to 90°S. Cl activation for the total Cly in 2012 shows a sharp transition at 195 K (Fig. 5F), which matches remarkably well with the current understanding of Cl activation on PSCs as first observed with aircraft methods (15). It

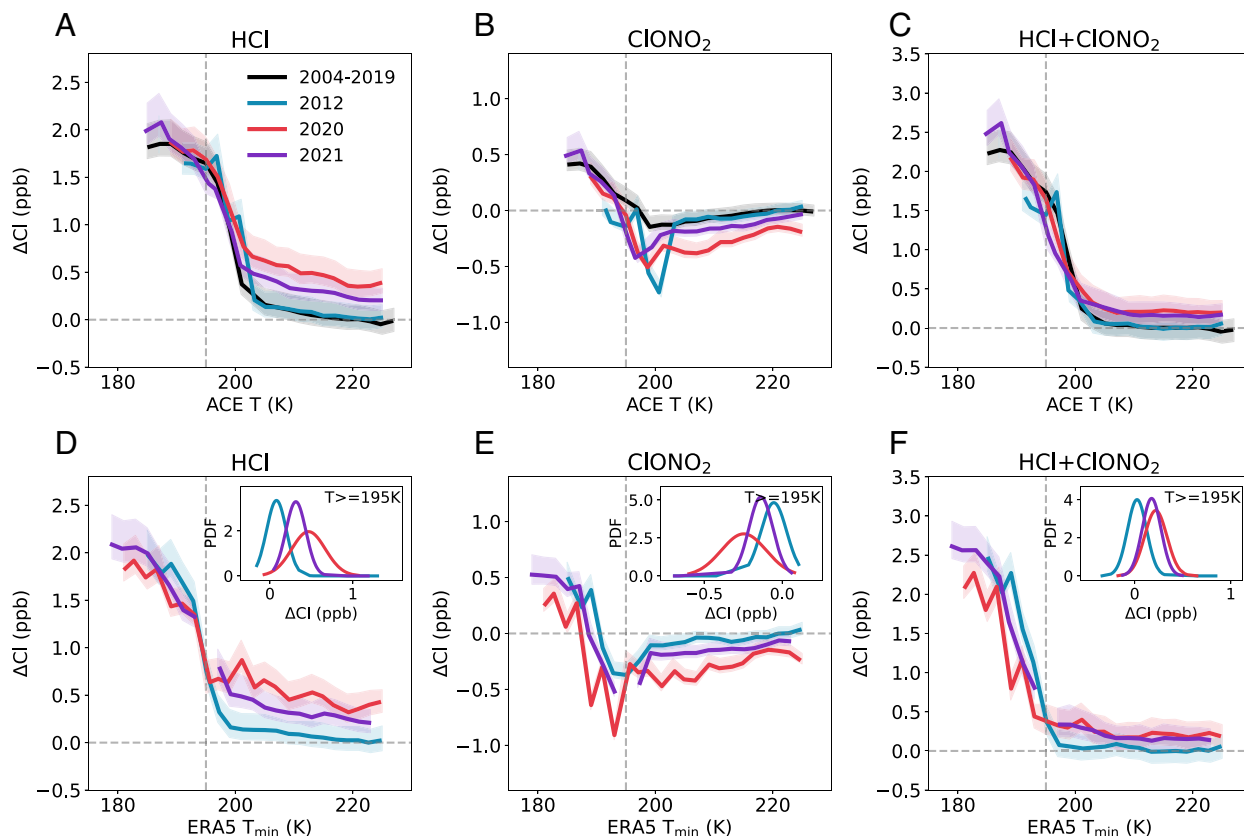


Fig. 5. Cl activation as a function of temperature in the polar vortex region (65 to 90°S), as in Fig. 4 for midlatitudes. Panels A–C use the ACE-measured temperature at the satellite overpass, and panels D–F use the minimum temperature (T_{\min}) calculated along the 5-d back trajectories for each data point for 2020, 2021, and 2012.

is noteworthy that even in 2012 when the background CO and aerosol extinctions are at the lower end in the climatology, there is still some ClONO₂ being converted from HCl at temperatures between 195 and 200 K (Fig. 5 D and E). Observations show that organic aerosols are widespread in the lower stratosphere. Among other sources, tropical biomass burning produces organic aerosols in the upper troposphere (33) that may be transported into the stratosphere. Thus, early season Cl processing on organic aerosols could occur to some extent every year, albeit with smaller magnitudes than in 2020.

Data in 2020 and 2021 show that a similar Cl processing mechanism also took place in the south polar vortex region at temperatures above 195 K. HCl in 2020 and 2021 continues to indicate more active Cl compared to other years at all temperatures until the temperature falls below 195 K, when the PSCs likely dominate the Cl activation, and these 2 y merge into the 2004 to 2019 climatology. While Cl activation in 2020 was lower at temperatures well below 195 K (Fig. 5F) compared to other years, this does not necessarily mean less total active Cl being present in that year (e.g., there could also be an interannual variability in the total Cl). In particular, the results show that a large amount of Cl has already been activated earlier in the season (at warmer temperatures) and likely stayed in the forms of HOCl, ClO, and Cl₂O₂ in the polar vortex region (6, 7). Because of less solar radiation at higher latitudes, less NO₂ is available from HNO₃ photochemistry to transfer these more reactive forms of Cl back to ClONO₂. This is supported by the evidence of large nonzero values of the mean of PDFs for ΔHCl+ClONO₂ at temperatures above 195 K in Fig. 5F (0.22 ± 0.12 ppb in 2020 and 0.18 ± 0.10 ppb in 2021, compared to 0.02 ± 0.10 ppb in 2012; ± sign followed by one SD).

Note that most of the ACE data points in the polar region are over 65 to 70°S (especially in colder seasons) and may not

represent the conditions in the core of the polar vortex. *SI Appendix, Fig. S8* shows the limited data available for Cl activation between 70 and 90°S (ACE observations for March and April only). The general behavior of Cl processing at warmer temperatures remains apparent in these months at high latitudes.

Altitude-Dependent Cl Activation in the Polar Vortex Region.

The reaction efficiency of HCl+ClONO₂ can be affected not only by different types of surfaces (e.g., organic aerosols and PSCs), but also by water vapor content and pressure, which vary with altitude (34), which has been suggested as a potential midlatitude ozone depletion mechanism (35, 36). We therefore expand the focus to the range of altitudes from 14.5 to 18.5 km for 2020, 2021, and 2012 (Fig. 6). The number of datapoints (after filtering by the data quality flag) is similar between 14.5 and 18.5 km, but it has dropped by more than 50% at below 13 km; thus altitudes below 14.5 km have been discarded.

It is noteworthy that in a year without the impact of organic aerosols from large wildfires (2012), a systematic gradient of the onset temperature for Cl activation is indicated, from 200 K at 14.5 km to 195 K at 18.5 km using the 5-d back trajectories (Fig. 6A). This agrees surprisingly well with current understanding, as indicated by a numerical calculation using the kinetics code and composition data from Whole Atmosphere Community Climate Model (WACCM) (14). For example, the reaction efficiency for HCl+ClONO₂ is about 80 times more efficient at 14.5 km than at 18.5 km (*SI Appendix, Fig. S9B*), suggesting Cl activation can happen at warmer temperatures much more readily at 14.5 km than at 18.5 km. But such altitude dependency is significantly disturbed by organic aerosols after the 2020 Australian wildfire. Neither 2020 nor 2021 demonstrate a clear relationship between Cl activation and

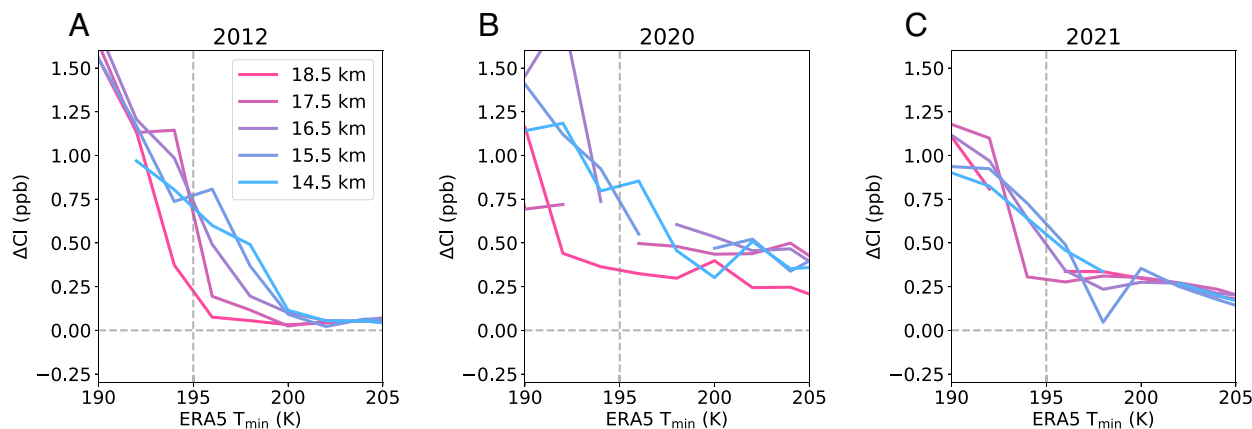


Fig. 6. The altitude-dependent Cl activation in the polar vortex region (65 to 90°S) for (A) 2012, (B) 2020, and (C) 2021. The x axis shows the minimum temperature calculated along the 5-d back trajectories, and the y axis shows the Cl activation from the sum of HCl and ClONO₂. Only the Cl activation calculated from baselines using all available data from 2004 to 2019 is shown here. Each line represents a different altitude range from 14.5 to 18.5 km. The panels are zoomed in for 190 to 205 K to focus on the onset temperature for Cl activation on PSCs.

altitude. Instead, large amounts of Cl activation took place at all altitudes ranging from 14.5 to 18.5 km in these years at temperatures warmer than 195 K.

Discussion

In conclusion, we have examined the HCl and ClONO₂ reservoir species that reflect heterogeneous reactions in the southern hemisphere fall and winter (March to July) for both the Australian wildfire-released organic aerosols and background conditions using satellite data. Our method confirms a sharp increase in Cl activation for temperatures below about 195 K along 5-d air parcel trajectories characterizing the data, consistent with current understanding for Cl activation in the polar region (11, 16, 37). This finding highlights the importance of relatively small temperature perturbations (i.e., less than 1 K) on this chemistry (e.g., those due to planetary or gravity waves) for air parcels with low temperatures but not low enough to trigger heterogeneous reactions. The method also successfully demonstrates the altitude dependency of Cl activation for a reference non-wildfire year (34). These results illustrate the power of this method for both background conditions and wildfire perturbations in testing chemical understanding.

We find evidence for Cl processing at much warmer temperatures (at 220 K) in both midlatitude and polar vortex regions after the Australian fires than the current understanding for PSCs, which is essentially limited to polar region at temperatures below 195 K. When such Cl processing happens at midlatitudes, HCl decreases but nearly all of the active Cl is turned into ClONO₂ rapidly because of ongoing supply of NO₂ from HNO₃ photolysis and reaction with OH. However, PDFs of the sum of HCl+ClONO₂ activation reveal that some enhanced Cl does remain in active forms at temperatures above 195 K in 2020, which can be expected to produce some ozone loss. Importantly, the data suggest that the remaining aerosols from the 2020 wildfire apparently even continued to affect the Cl species (albeit to a lesser extent) into 2021. Further, diversity in wildfire-released organic aerosols (17, 18) with different chemical properties is suggested by an observed increase in the width of the distribution, i.e., varying amounts of Cl activation.

The total Cl budget could be closed by including other species, particularly ClO and Cl₂O₂. However, one drawback of this tracer–tracer method is that it works well for the rather long-lived species (e.g., HCl and ClONO₂), but the large variance in more short-lived species (e.g., ClO and HOCl) can impede the calculation. Furthermore, the ACE satellite produces twilight measurements (which do not indicate daytime ClO values) and it does

not have measurements for Cl₂O₂; although (6) shows enhanced daytime ClO using MLS data, and twilight ClO enhancement is also found from ACE data albeit with larger noise (7). HNO₃ is not taken up by the organic aerosols, and reported midlatitude HNO₃ in 2020 is within the climatological variance (6). However, PSCs do take up HNO₃ in the polar region (therefore reducing NO_x, impacting the Cl₂ reservoirs). But ACE does not monitor inside the polar vortex during dark conditions. Further studies are needed to evaluate the total Cl budget and to fully quantify to what extent the ozone layer is affected by wildfire-triggered Cl processing.

The frequency of wildfires is projected to increase in the future due to climate change (38). A better understanding of the range of composition of organic aerosols, and of heterogeneous reaction rates upon them, is needed to estimate any associated ozone impacts, including potential delay of the recovery in the stratospheric ozone layer in Antarctica, as well as potential midlatitude ozone loss in the future.

Materials and Methods

Satellite Datasets. Level 2 satellite data from Atmospheric Chemistry Experiment–Fourier Transform Spectrometer (ACE-FTS) version 4.1 for molecules (39) is used in this study. Data range from 2004 to 2021. ACE provides measurements at twilight; both the sunrise and sunset data are used. We remove outliers defined as three SDs apart from the mean for each month (40).

Daily level 3 satellite data from Microwave Limb Sounder (MLS) version 5.0 (41) for N₂O, HCl and temperature are used in this study. Data range from 2005 to 2021. Both the ascending and descending modes are used, which provide measurements for daytime and nighttime.

Back Trajectory Calculation. Lagranto (Lagrangian Analysis Tool) version 2.0 (22) is used in this study to calculate the kinematic back trajectories for each data point in 2020, 2021, and 2012. It iterates three times in each time interval to calculate the average velocity between the starting and ending locations (from every iteration). Lagranto is driven by the ERA5 reanalysis data (fifth generation atmospheric reanalysis product from the European Centre for Medium-Range Weather Forecasts) (23) for pressure, temperature, and 3D (three-dimensional) wind fields. We used an ERA5 configuration that has 137 vertical model levels, a 1° horizontal resolution, and a 3-h temporal resolution. Subgrid-scale gravity waves can introduce temperature variability. ERA5 has been shown to resolve a large portion of that variability (42–44) and will be sampled irrespective of the time interval chosen for transport in the trajectory model. However, short horizontal wavelength disturbances could lead to effective chlorine activation at somewhat colder temperatures than those shown here, which should be considered an upper limit to the activation temperature.

HCl+ClONO₂ Reaction Efficiency. The HCl+ClONO₂ reactive uptake probabilities (in *SI Appendix, Fig. S9B*) are calculated using the parameterization described in ref. 14, which is used in the WACCM model. This calculation uses model values of temperature and pressure over an altitude range of 14.5 to 19.5 km during July at ~63°S. HCl and ClONO₂ volume mixing ratios are held constant at 0.3 and 0.05 ppb, respectively. Water vapor volume mixing ratio is held constant at 3.5, 4, and 4.5 ppm. This allows for the effect of water vapor partial pressure over the above altitude to range to be investigated.

Data, Materials, and Software Availability. Data and code used in this study are available at <https://doi.org/10.5281/zenodo.7504238> (45).

ACKNOWLEDGMENTS. We appreciate Hongwei Sun (Harvard University) for the guidance in using Lagranto. P.W., S.S., and K.S. gratefully acknowledge partial support by NSF-1906719 and NASA 80NSSC19K0952. We thank P. F. Bernath, Mission Scientist of the Atmospheric Chemistry Experiment. ACE is supported by the Canadian Space Agency (which makes ACE data freely available).

1. D. A. Peterson *et al.*, Australia's black summer pyrocumulonimbus super outbreak reveals potential for increasingly extreme stratospheric smoke events. *NPJ Clim. Atmos. Sci.* **4**, 38 (2021).
2. G. D'Angelo, S. Guimond, J. Reisinger, D. A. Peterson, M. Dubey, Contrasting stratospheric smoke mass and lifetime from 2017 Canadian and 2019/2020 Australian megafires: Global simulations and satellite observations. *J. Geophys. Res. Atmos.* **127**, e2021JD036249 (2022).
3. T. Deshler *et al.*, Trends in the nonvolcanic component of stratospheric aerosol over the period 1971–2004. *J. Geophys. Res.* **111**, D01201 (2006).
4. P. Yu *et al.*, Persistent stratospheric warming due to 2019–2020 Australian wildfire smoke. *Geophys. Res. Lett.* **48**, e92609 (2021).
5. L. A. Rieger, W. J. Randel, A. E. Bourassa, S. Solomon, Stratospheric temperature and ozone anomalies associated with the 2020 Australian new year fires. *Geophys. Res. Lett.* **48**, e2021GL095898 (2021).
6. M. L. Santee *et al.*, Prolonged and pervasive perturbations in the composition of the Southern Hemisphere midlatitude lower stratosphere from the Australian new year's fires. *Geophys. Res. Lett.* **49**, e2021GL096270 (2022).
7. P. Bernath, C. Boone, J. Crouse, Wildfire smoke destroys stratospheric ozone. *Science* **375**, 1292–1295 (2022).
8. A. R. Klekociuk *et al.*, The Antarctic ozone hole during 2020. *J. South. Hemisph. Earth Syst. Sci.* **72**, 19–37 (2022).
9. A. Ansmann *et al.*, Ozone depletion in the Arctic and Antarctic stratosphere induced by wildfire smoke. *Atmos. Chem. Phys.* **22**, 11701–11726 (2022).
10. S. E. Strahan *et al.*, Unexpected repartitioning of stratospheric inorganic chlorine after the 2020 Australian wildfires. *Geophys. Res. Lett.* **49**, e98290 (2022).
11. S. Solomon, R. R. Garcia, F. S. Rowland, D. J. Wuebbles, On the depletion of Antarctic ozone. *Nature* **321**, 755–758 (1986).
12. S. Solomon *et al.*, On the stratospheric chemistry of midlatitude wildfire smoke. *Proc. Natl. Acad. Sci. U.S.A.* **119**, e2117325119 (2022).
13. D. R. Hanson, A. R. Ravishankara, Uptake of hydrochloric acid and hypochlorous acid onto sulfuric acid: Solubilities, diffusivities, and reaction. *J. Phys. Chem.* **97**, 12309–12319 (1993).
14. Q. Shi, J. T. Jayne, C. E. Kolb, D. R. Worsnop, P. Davidovits, Kinetic model for reaction of ClONO₂ with H₂O and HCl and HOCl with HCl in sulfuric acid solutions. *J. Geophys. Res.* **106**, 24259–24274 (2001).
15. S. R. Kawa *et al.*, Activation of chlorine in sulfate aerosol as inferred from aircraft observations. *J. Geophys. Res.* **102**, 3921–3933 (1997).
16. S. Solomon, D. Kinnison, J. Bandoro, R. Garcia, Simulation of polar ozone depletion: An update. *J. Geophys. Res. Atmos.* **120**, 7958–7974 (2015).
17. C. D. Boone, P. F. Bernath, M. D. Fromm, Pyrocumulonimbus stratospheric plume injections measured by the ACE-FTS. *Geophys. Res. Lett.* **47**, e2020GL088442 (2020).
18. D. M. Murphy *et al.*, Radiative and chemical implications of the size and composition of aerosol particles in the existing or modified global stratosphere. *Atmos. Chem. Phys.* **21**, 8915–8932 (2021).
19. J. R. Lawrence, S. V. Glass, S.-C. Park, G. M. Nathanson, Surfactant control of gas uptake: Effect of butanol films on HCl and HBr entry into supercooled sulfuric acid. *J. Phys. Chem. A* **109**, 7458–7465 (2005).
20. Y. Q. Li *et al.*, Uptake of HCl(g) and HBr(g) on ethylene glycol surfaces as a function of relative humidity and temperature. *J. Phys. Chem. A* **106**, 1220–1227 (2002).
21. P. F. Bernath, Atmospheric Chemistry Experiment (ACE): Mission overview. *Geophys. Res. Lett.* **32**, L15S01 (2005).
22. M. Sprenger, H. Wernli, The LAGRANTO Lagrangian analysis tool—Version 2.0. *Geosci. Model Dev.* **8**, 2569–2586 (2015).
23. H. Hersbach *et al.*, The ERA5 global reanalysis. *Q. J. R. Meteorol. Soc.* **146**, 1999–2049 (2020).
24. M. P. Chipperfield *et al.*, On the use of HF as a reference for the comparison of stratospheric observations and models. *J. Geophys. Res.* **102**, 12901–12919 (1997).
25. S. Tilmes, R. Müller, J.-U. GroöB, J. M. Russell III, Ozone loss and chlorine activation in the Arctic winters 1991–2003 derived with the tracer-tracer correlations. *Atmos. Chem. Phys.* **4**, 2181–2213 (2004).
26. M. H. Proffitt, S. Solomon, M. Loewenstein, Comparison of 2-D model simulations of ozone and nitrous oxide at high latitudes with stratospheric measurements. *J. Geophys. Res.* **97**, 939 (1992).
27. M. H. Proffitt *et al.*, Ozone loss in the Arctic polar vortex inferred from high-altitude aircraft measurements. *Nature* **347**, 31–36 (1990).
28. D. Griffin *et al.*, Stratospheric ozone loss in the Arctic winters between 2005 and 2013 derived with ACE-FTS measurements. *Atmos. Chem. Phys.* **19**, 577–601 (2019).
29. N. J. Livesey *et al.*, Investigation and amelioration of long-term instrumental drifts in water vapor and nitrous oxide measurements from the Aura Microwave Limb Sounder (MLS) and their implications for studies of variability and trends. *Atmos. Chem. Phys.* **21**, 15409–15430 (2021).
30. M. P. Chipperfield, E. R. Lutman, J. A. Kettleborough, J. A. Pyle, A. E. Roche, Model studies of chlorine deactivation and formation of ClONO₂ collar in the Arctic polar vortex. *J. Geophys. Res.* **102**, 1467–1478 (1997).
31. D. L. Hartmann, J. R. Holton, Q. Fu, The heat balance of the tropical tropopause, cirrus, and stratospheric dehydration. *Geophys. Res. Lett.* **28**, 1969–1972 (2001).
32. M. G. Mlynczak, C. J. Mertens, R. R. Garcia, R. W. Portmann, A detailed evaluation of the stratospheric heat budget: 2. Global radiation balance and diabatic circulations. *J. Geophys. Res.* **104**, 6039–6066 (1999).
33. G. P. Schill *et al.*, Widespread biomass burning smoke throughout the remote troposphere. *Nat. Geosci.* **13**, 422–427 (2020).
34. S. Solomon, Stratospheric ozone depletion: A review of concepts and history. *Rev. Geophys.* **37**, 275–316 (1999).
35. J. G. Anderson *et al.*, Stratospheric ozone over the United States in summer linked to observations of convection and temperature via chlorine and bromine catalysis. *Proc. Natl. Acad. Sci. U.S.A.* **114**, E4905–E4913 (2017).
36. C. E. Clapp, J. G. Anderson, Modeling the effect of potential nitric acid removal during convective injection of water vapor over the Central United States on the chemical composition of the lower stratosphere. *J. Geophys. Res. Atmos.* **124**, 9743–9770 (2019).
37. D. M. Wilmouth *et al.*, Evolution of inorganic chlorine partitioning in the Arctic polar vortex. *J. Geophys. Res.* **111**, D16308 (2006).
38. S. I. Senéviratne, *et al.*, "Chapter 11: Weather and climate extreme events in a changing climate" (IPCC sixth assessment report, WMO/UNEP, Cambridge University Press, Cambridge, United Kingdom and New York, NY, 2021).
39. C. D. Boone *et al.*, Retrievals for the atmospheric chemistry experiment Fourier-transform spectrometer. *Appl. Opt.* **44**, 7218 (2005).
40. C. Boone Data usage guide and file format description for ACE-FTS level 2 data version 4.1 ASCII format (2020). Department of Chemistry, University of Waterloo, Waterloo, Ontario, Canada. (August 2, 2022).
41. N. Livesey, Version 5.0x level 2 and 3 data quality and description document. Jet Propulsion Laboratory, Pasadena, USA. (2022).
42. A. Dörnbrack, S. D. Eckermann, B. P. Williams, J. Haggerty, Stratospheric gravity waves excited by a propagating Rossby wave train—A DEEPWAVE case study. *J. Atmos. Sci.* **79**, 567–591 (2022).
43. A. Dörnbrack *et al.*, Unusual appearance of mother-of-pearl clouds above El Calafate, Argentina (50°21'S, 72°16'W). *Weather* **75**, 378–388 (2020).
44. A. Dörnbrack, Stratospheric mountain waves trailing across Northern Europe. *J. Atmos. Sci.* **78**, 2835–2857 (2021).
45. P. Wang, S. Solomon, K. Stone, Data and code for "Stratospheric chlorine processing after the 2020 Australian wildfires derived from satellite data" (2022). Zenodo. <https://doi.org/10.5281/zenodo.7504238>. Deposited 5 August 2022.